

Redox-dependent conformational changes in eukaryotic cytochromes revealed by paramagnetic NMR spectroscopy

Alexander N. Volkov · Sophie Vanwetswinkel ·
Karen Van de Water · Nico A. J. van Nuland

Received: 6 November 2011 / Accepted: 15 January 2012 / Published online: 10 February 2012
© Springer Science+Business Media B.V. 2012

Abstract Cytochrome *c* (Cc) is a soluble electron carrier protein, transferring reducing equivalents between Cc reductase and Cc oxidase in eukaryotes. In this work, we assessed the structural differences between reduced and oxidized Cc in solution by paramagnetic NMR spectroscopy. First, we have obtained nearly-complete backbone NMR resonance assignments for *iso*-1-yeast Cc and horse Cc in both oxidation states. These were further used to derive pseudocontact shifts (PCSs) arising from the paramagnetic haem group. Then, an extensive dataset comprising over 450 measured PCSs and high-resolution X-ray and solution NMR structures of both proteins were used to define the anisotropic magnetic susceptibility tensor, $\Delta\chi$. For most nuclei, the PCSs back-calculated from the $\Delta\chi$ tensor are in excellent agreement with the experimental PCS values. However, several contiguous stretches—clustered around G41, N52, and A81—exhibit large deviations both in yeast and horse Cc. This behaviour is indicative of redox-dependent structural changes, the extent of which is likely conserved in the protein family. We propose that the observed discrepancies arise from the changes in protein dynamics and discuss possible functional implications.

Electronic supplementary material The online version of this article (doi:10.1007/s10858-012-9607-8) contains supplementary material, which is available to authorized users.

A. N. Volkov · S. Vanwetswinkel · K. Van de Water ·
N. A. J. van Nuland (✉)
Jean Jeener NMR Centre, Structural Biology Brussels,
Vrije Universiteit Brussel, Pleinlaan 2, 1050 Brussels, Belgium
e-mail: nvnuland@vub.ac.be

A. N. Volkov · S. Vanwetswinkel · K. Van de Water ·
N. A. J. van Nuland
Department of Structural Biology, VIB, Pleinlaan 2,
1050 Brussels, Belgium

Keywords Cytochrome *c* · Paramagnetic NMR ·
Protein dynamics · Pseudocontact shifts

Introduction

Cytochrome *c* (Cc) is a key component of the eukaryotic respiratory chain, where it functions as an electron carrier between the membrane-bound Cc reductase and Cc oxidase. In yeast, Cc has other physiological partners, such as cytochrome *b*₂ (also known as lactate dehydrogenase) and cytochrome *c* peroxidase (Banci and Assfalg 2001). The primary sequence of this protein, reported for more than 100 different species, is highly conserved among eukaryotes (Banci and Assfalg 2001). Two isoforms, *iso*-1 and *iso*-2, are found in yeast, the former of which is much more widely studied and is referred to as yCc in this work. yCc is a positively-charged (pI = 9.54), low molecular weight (12.7 kDa) protein, consisting of 108 amino-acids and the haem prosthetic group.¹

Cc is nearly spherical in shape and is formed by five α -helices and a short β -strand, an overall fold that is highly conserved across the protein family (Banci et al. 1999b; Banci and Assfalg 2001). The protein contains a *c*-type haem group located near the N-terminus and attached to the polypeptide chain by covalent thioether bonds with two cysteine residues, C14 and C17, from the canonical CXXCH sequence. The haem harbours a six-coordinated iron atom that has two physiologically relevant oxidation states, Fe(II) and Fe(III), and is diamagnetic in the ferrous and paramagnetic in the ferric form. The coordination

¹ The amino-acid numbering for yCc used in this work is based on the sequence alignment with horse heart Cc (hCc), which generates a negative numbering for the first five residues.

sphere consists of four pyrrole nitrogens of the haem, the $N_{\epsilon 2}$ atom of H18, and the S_{δ} atom of M80. To date, a number of high-resolution X-ray and solution NMR structures of cytochromes *c* from different species have been reported (Banci and Assfalg 2001).

Overall, the three-dimensional structures of the reduced (Cc^{red}) and oxidized (Cc^{ox}) proteins are highly similar (see Table 4 for the PDB entries and references). However, solution NMR studies of yCc revealed slight conformational changes between the two redox states, such as re-organization of the hydrogen bond network involving one of the haem propionates and a concomitant reorientation of the N52 side-chain (Baistrocchi et al. 1996; Banci et al. 1997a). In addition, NMR studies of yCc by hydrogen–deuterium (HD) exchange spectroscopy (Banci et al. 1997a; Baxter and Fetrow 1999) and relaxation techniques (Fetrow and Baxter 1999) showed that yCc^{ox} is more flexible than yCc^{red}. At present, it is not clear whether the redox-dependent rearrangement of the haem-centred H-bond network and differences in protein dynamics play a functional role in the modulation of the macromolecular recognition or electron transfer rates in Cc complexes (Banci et al. 2000).

In order to gain a deeper insight into the nature and extent of the proposed redox-dependent structural changes of Cc in solution, we used paramagnetic NMR spectroscopy. Presence of paramagnetic species with an anisotropic magnetic susceptibility tensor, $\Delta\chi$, gives rise to pseudo-contact shifts (PCS), readily detectable as the difference in chemical shifts of the protein resonances in the oxidized and reduced forms (Ubbink et al. 2002). The PCS depends on the position of the observed nucleus in the $\Delta\chi$ reference frame. For a protein of known structure, the latter can be determined from experimental PCSs measured for multiple nuclei, thus providing the asymmetry, magnitude, and the orientation of the $\Delta\chi$ tensor. Once the $\Delta\chi$ reference frame is known, a PCS value can be calculated for every atom in the protein molecule. For rigid systems exhibiting no structural differences between the oxidized and reduced states, the experimental PCSs are exactly equal to the PCS values back-calculated from the determined $\Delta\chi$ tensor. Discrepancies between the two datasets, however, might

indicate the presence of additional contributions arising from redox-dependent structural changes (Feng et al. 1990; Williams et al. 1985).

In this work, we have obtained nearly-complete NMR assignments of HN, N, CO, C_{α} and C_{β} resonances of the oxidized and reduced Cc from yeast and horse and used those in the $\Delta\chi$ tensor calculations. The magnitude and orientation of the $\Delta\chi$ tensors for both proteins are highly similar, which is not surprising given the high degree of sequence and structure conservation in the Cc protein family. For most of the nuclei, there is an excellent agreement between the experimental and back-calculated PCS values. However, several contiguous stretches of residues in both yeast and horse Cc exhibit large deviations. The affected areas map out onto a single patch of the protein structure, encompassing the haem propionate 7 group and a loop bearing the M80 ligand to the haem iron. We propose that the discrepancies in PCS values observed here arise from redox-dependent changes in protein dynamics.

Results and discussion

NMR assignments of yCc and hCc

Here, we report nearly complete assignments of HN, N, C_{α} , and C_{β} resonances of yCc and hCc in both oxidation states (Table 1). For yCc, the backbone amide resonances of G83 (yCc^{ox}), G84 (yCc^{red}) and the C_{β} resonance of T96 (yCc^{ox}/yCc^{red}) were not observed. In the X-ray structures of yCc and hCc (see Table 4 for details), the HN atom of G84 is located close to the centre of the F82 phenyl ring, a favourable geometry for an amide-aromatic hydrogen bond (Levitt and Perutz 1988). Such an arrangement would lead to a strong, upfield shift of the G84 HN resonance due to the ring-current effect of F82. Indeed, a chemical shift of 4.6 ppm was observed for G84 HN nucleus of hCc in an earlier work (Liu et al. 2003). Except for yCc^{ox} with G84 HN assigned to a peak at 4.9 ppm, here we failed to detect this resonance, likely due to an overlap with the dominant water peak at 4.7 ppm. In addition to G84 HN, the hCc

Table 1 Extent of backbone resonance assignment (in %) for yCc and hCc performed in 20 mM sodium phosphate 0.1 M NaCl, pH 6.0 at 303 K. The residues for which no assignments were obtained are given in parentheses

	yCc ^{ox}	yCc ^{red}	hCc ^{ox}	hCc ^{red}
NH	99.0 (G83)	99.0 (G84)	97.0 (E21, T28, G84)	98.0 (E21, G84)
CO	89.8 (A-5, L9, <i>G24</i> , P25, <i>G29</i> , N70, I75, F82, K86, L94, E103)	92.6 (E21, <i>G24</i> , <i>G29</i> , Q42, N70, I75, G83, E103)	88.5 (V20, K27, <i>G29</i> , L32, R38, A43, E66, N70, I75, A83, K86, E104)	91.3 (V20, K25, <i>G29</i> , A43, N70, I75, A83, G84, E104)
C_{α}	100	100	100	100
C_{β}	99.0 (T96)	99.0 (T96)	100	100

In italic are the residues whose CO resonances cannot be assigned from the HNCO experiment (see text)

resonances of E21 HN (hCc^{ox}/hCc^{red}) and T28 HN (hCc^{ox}) were not observed here, consistent with earlier work (Liu et al. 2003).

We have not pursued the complete assignment of backbone carbonyl resonances, but rather aimed at generating a sufficiently large dataset for the $\Delta\chi$ tensor calculations (see below). To this end, only an HNCO spectrum was acquired. As a result, no assignments of CO resonances for the C-terminal residue or the residues followed by a proline or by a residue with an unassigned NH peak could be made (italicized in Table 1). Besides, a number of CO resonances could not be assigned due to spectral overlap.

In addition to the backbone nuclei, we have also assigned all heavy sidechain-atoms of Asn and Gln residues, except for C_γ atoms of N31 (yCc^{ox}/yCc^{red} , hCc^{ox}) and N52 (yCc^{red}). For all systems studied, the HSQC spectra acquired at low and high ionic strengths are essentially identical, except for several backbone amide resonances of charged amino-acids exhibiting salt-induced shifts (Fig. S1). Overall, yCc appears to be more sensitive to salt than hCc , which agrees well with the findings of an earlier 1D 1H study (Moench et al. 1991).

The assignments of the backbone amide protons of yCc obtained in this work are in excellent agreement with those reported by Gao et al. 1990 (Fig. 1a). The only discrepancies are found for the HN atoms of K79 in the reduced and M80 in the oxidized form (outliers in Fig. 1a). The latter assignment was later corrected to 8.86 ppm (Banci et al. 1997a), closely matching the value obtained in this work. For the backbone amide nitrogen atoms, a number of differences are observed between the present and the published datasets (Fig. 1b). As N nuclei are highly sensitive to variations in the sample composition, most of the

discrepancies can be attributed to differences in the experimental conditions: 50 mM sodium acetate pH 4.6 used in earlier reports (Fetrow and Baxter 1999; Morar et al. 1999) and 20 mM sodium phosphate 0.1 M NaCl pH 6.0 in this work. However, several N resonances might have been erroneously assigned in previous reports, which used 3D NOESY-HSQC (Fetrow and Baxter 1999) or unspecified experiments (Morar et al. 1999). In principle, unambiguous assignments of backbone amide resonances cannot be derived from NOESY-HSQC spectra alone and require a complementary experiment, such as TOCSY-HSQC (Rule and Hitchens 2006).

For example, the published assignments of N atoms of G23 and I75 in yCc^{ox} appear to be swapped (Fetrow and Baxter 1999; Morar et al. 1999). A possible explanation for this discrepancy is an ambiguity in sequential HN–HN NOE connectivities as illustrated in Fig. 2. The HN resonances of Y74 ($i - 1$ residue of I75) and G24 ($i + 1$ residue of G23) have nearly the same proton frequency, making it difficult to distinguish between the correct I75–Y74/G23–G24 and an erroneous I75–G24/G23–Y74 connections (Fig. 2). Residues I75 and G24 are followed by prolines, precluding verification of the tentative assignments through HN_i/HN_{i+1} connectivities. In addition, the NOE cross-peak between HN atoms of G23 and K22 is very weak (not seen at the noise level in Fig. 2). Judging from the signal-to-noise level of the NOESY-HSQC spectrum (Fig. 2 in Fetrow and Baxter 1999), this cross-peak would not be detected in the previous work and, thus, could not be used to verify the G23 HN assignment. Given the lower resolution and signal-to-noise ratio in the spectra of Fetrow and Baxter (acquired at 500 MHz as compared to 800 MHz used in this report), it seems unlikely that the unambiguous assignments of the sequential connections in

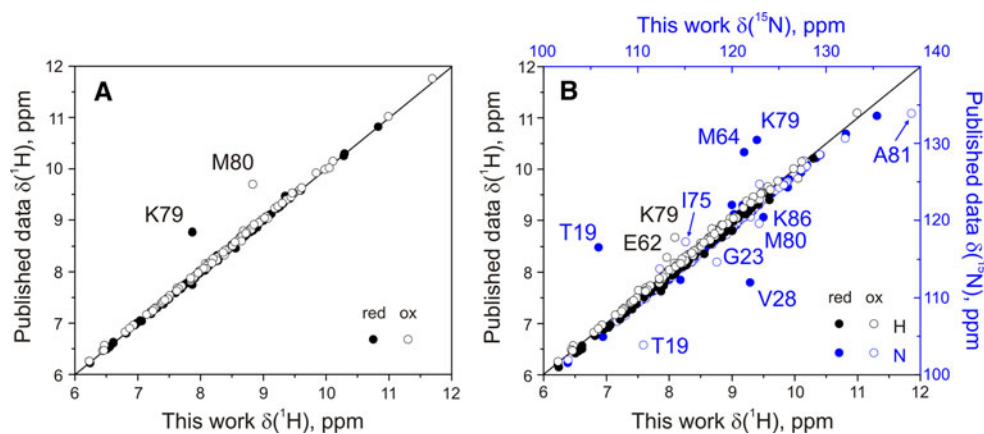


Fig. 1 Comparison of the backbone amide chemical shift assignments of yCc obtained in this and earlier works. **a** Chemical shifts of HN atoms of the reduced (filled circles) and oxidized (open circles) yCc as compared to the data of Gao et al. (BMRB entries 922 and 923, respectively; Gao et al. 1990). **b** Chemical shifts of HN (black)

and N (blue) atoms of the reduced (filled circles) and oxidized (open circles) yCc as compared to the data of Fetrow and Baxter (Fetrow and Baxter 1999). The most prominent outliers are indicated by the labels

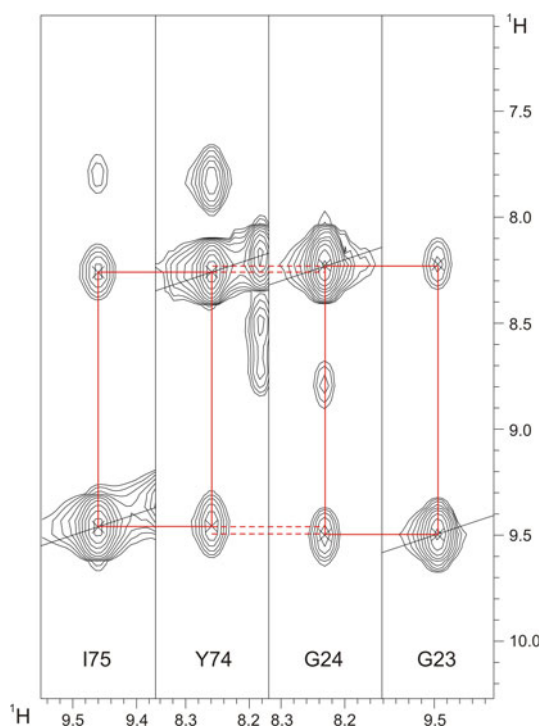


Fig. 2 Selected ^1H - ^1H planes of the ^{15}N -NOESY-HSQC spectrum of yCc^{Ox} . Solid red lines identify sequential HN-HN cross-peaks. Dashed lines indicate a possible ambiguity, connecting I75-G24 and G23-Y74 pairs of residues

I75-Y74 and G24-G23 pairs could be made in that work (Fetrow and Baxter 1999). Here, the ambiguity has been resolved through the combined use of HNCACB and CBCA(CO)NH experiments.

The assignments of backbone atoms of hCc obtained in this work are in excellent agreement with the published data (Fig. S2a; Liu et al. 2003). Comparison of the assignments for C_α , C_β , and CO resonances of wt hCc (used in this work) with those of the H26 N/H33 N hCc variant (Liu et al. 2003) reveals a remarkable similarity (Fig. S2b), confirming that the introduced mutations do not perturb the structure of the protein. (Liu et al. 2003).

Pseudocontact shifts and $\Delta\chi$ -tensor calculations

The chemical shift of a given nucleus in the oxidized, paramagnetic form (δ_{Ox}) can be expressed as:

$$\delta_{\text{Ox}} = \delta_{\text{red}} + \delta_{\text{CS}} + \delta_{\text{PCS}} + \Delta\delta_{\text{struct}} + \Delta\delta_{\text{other}}, \quad (1)$$

where δ_{red} is the chemical shift of the nucleus in the reduced, diamagnetic form; δ_{CS} and δ_{PCS} are the contact and pseudocontact shifts; $\Delta\delta_{\text{struct}}$ is the chemical shift contribution arising from the redox-dependent structural changes; and $\Delta\delta_{\text{other}}$ is the term combining all other differences in the chemical shifts, for example those arising

from slight discrepancies in the experimental conditions of the reduced and oxidized samples. In the absence of the contact shifts, which are only observed for the groups of atoms in direct contact with or separated by a few covalent bonds from the paramagnetic centre (Ubbink et al. 2002), the difference between the chemical shifts in the oxidized and reduced forms ($\Delta\delta_{\text{obs}}$) is given by (2):

$$\Delta\delta_{\text{obs}} = \delta_{\text{Ox}} - \delta_{\text{red}} = \delta_{\text{PCS}} + \Delta\delta_{\text{struct}} + \Delta\delta_{\text{other}} \quad (2)$$

If the system undergoes no redox-dependent structural changes and the experimental conditions of the reduced and oxidized samples closely match, the last two terms in (2) become negligible, so that $\Delta\delta_{\text{obs}} \approx \delta_{\text{PCS}}$. Providing that the three-dimensional structure of the protein is known, a set of experimentally determined $\Delta\delta_{\text{obs}}$ values can be used in this case to determine the $\Delta\chi$ -tensor according to (3) in the “Experimental section”. With these assumptions in mind, we have used $\Delta\delta_{\text{obs}}$ datasets obtained in this work to calculate the $\Delta\chi$ tensors for yCc and hCc.

For yCc several subsets of nuclei were used in the $\Delta\chi$ tensor calculations (Table S1). Judging from the errors of the fitted parameters, the highest precision is achieved when an entire set of HN, N, C_α , C_β , and CO atoms is employed in the calculations. The magnitude and the orientation of the determined $\Delta\chi$ tensors are relatively insensitive to the choice of the input structure (Table S1). As signified by the lowest variance value, the best fit is obtained when the X-ray structure of yCc^{red} is used. The orientation of the determined $\Delta\chi$ tensor in the molecular frame of the protein is shown in Fig. 3, with the corresponding parameters presented in Table 2. With its origin at the haem iron, the $\Delta\chi$ reference frame deviates only slightly from the haem-centred coordinate system defined in Fig. 3b: the $\Delta\chi$ z' axis makes a 15° angle with the haem normal and the orthogonal x' and y' axes are rotated by 10° relative to the x and y axes of the molecular reference frame. The PCS isosurfaces of ± 0.5 ppm and ± 0.2 ppm span most of the protein, with only a small portion of each extending beyond the yCc surface (Fig. 3c). Thus, only a few intermolecular PCSs originating from yCc can be expected to be detected in its complexes with partner proteins.

The $\Delta\chi$ tensor parameters obtained in this work agree well with most of the values reported before (Table 2). Interestingly, the average parameters computed from four different yCc structures are strikingly similar to the $\Delta\chi$ tensor values of Gao et al. calculated from proton PCSs (Gao et al. 1991). The worst agreement is observed with the data of Banci et al., who used the NMR structure of yCc^{Ox} in the $\Delta\chi$ tensor calculations (Banci et al. 1997a). Despite similar values of the Euler angles, the $\Delta\chi_{\text{ax}}$ and $\Delta\chi_{\text{th}}$ obtained with the yCc^{Ox} NMR structure in this work

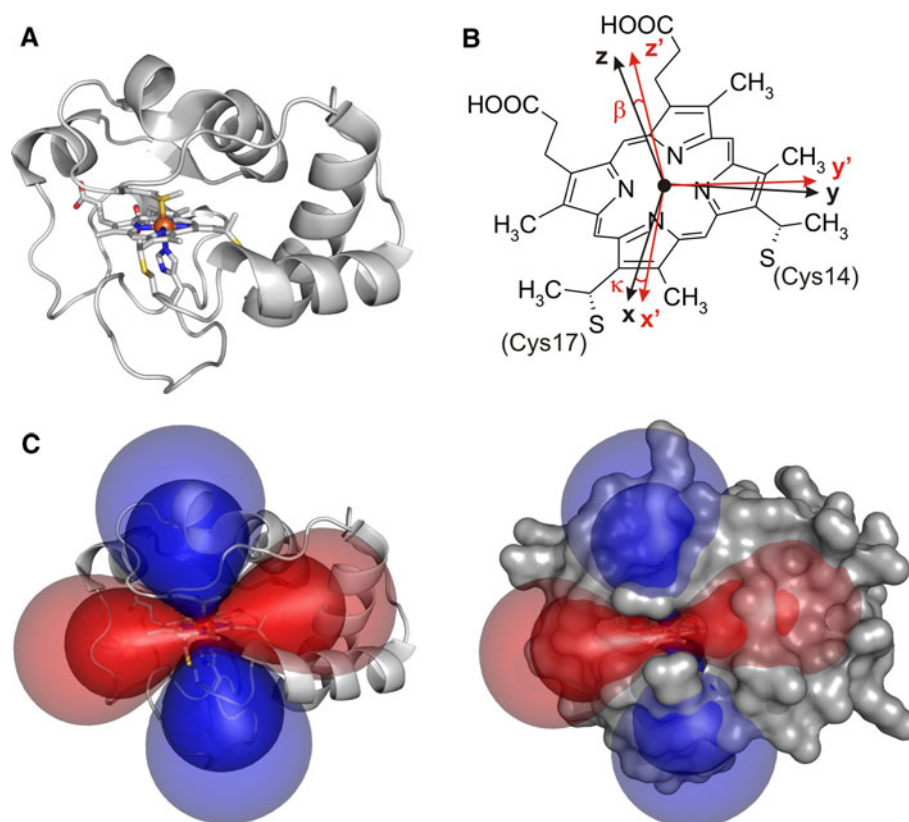


Fig. 3 Experimentally determined $\Delta\chi$ tensor of yCc. **a** The X-ray structure of yCc^{red} used for the tensor determination. The haem group and its ligands are shown as sticks, with iron atom as a sphere. **b** Definition of the molecular reference frame (black) and its relation to the principal axes of the $\Delta\chi$ tensor (red). The Euler angle β defines the cone angle between the haem normal and the tensor z' axis. At small β , as is the case here, the angle κ approximates the rotation of the orthogonal x' and y' axes relative to the molecular frame x and y

axes and can be expressed in terms of the other two $\Delta\chi$ Euler angles as $\kappa = (\alpha + \gamma) - \pi$. **c** PCS isosurfaces of ± 0.5 ppm (dark shade) and ± 0.2 ppm (light shade) in the molecular frame of yCc. The blue and red isosurfaces indicate positive and negative PCSs, respectively. The right panel displays the Van der Waals surface of yCc. The protein orientation is the same as in (a). PCS isosurfaces were calculated with Numbat (Schmitz et al. 2008). All molecular graphics in this work were prepared with PyMol (DeLano 2002)

Table 2 Comparison of $\Delta\chi$ tensors determined for yCc in this and earlier works. $\Delta\chi_{ax}$ and $\Delta\chi_{rh}$ are the axial and rhombic components of the $\Delta\chi$ tensor in units of 10^{-32} m³; β and κ are the angles (in degrees) relating the $\Delta\chi$ -tensor frame to the molecular coordinate system (Fig. 3b)

$\Delta\chi_{ax}$	$\Delta\chi_{rh}$	β	κ	Reference
3.17 ± 0.05	1.80 ± 0.09	15 ± 1	11 ± 2	This work ^a
3.06 ± 0.10	1.54 ± 0.17	14 ± 4	10 ± 3	This work ^b
3.01 ± 0.07	1.03 ± 0.12	11 ± 1	5 ± 3	(Worrall et al. 2001) ^a
3.33 ± 0.04	1.55 ± 0.04	6	20	(Sukits et al. 1997) ^a
2.22 ± 0.07	1.04 ± 0.07	17	9	(Banci et al. 1997a) ^c
3.06 ± 0.04	1.54 ± 0.05	9	6	(Gao et al. 1991) ^a

For details see Table S1 and the “Experimental section”

^a The X-ray structure of yCc^{red} was used in the calculations; ^b The reported values are the averages of $\Delta\chi$ parameters obtained from four yCc structures (Table S1); the errors are standard deviations; ^c The NMR structure of yCc^{ox} was used in the $\Delta\chi$ tensor determination

(Table S1) are significantly larger than those reported by Banci et al. (Banci et al. 1997a).

Contrary to the case of yCc, the calculation of the $\Delta\chi$ tensor for hCc is highly dependent on the input structure (Table S2), most likely due to significant differences

among the reported crystallographic and NMR structures. The best fit is achieved using the X-ray coordinates of hCc^{ox} (Table S2). The $\Delta\chi$ parameters obtained for hCc in this work lie in the range of previously reported values (Table 3), are very similar to those of yCc (Table 2), and

Table 3 Comparison of the $\Delta\chi$ tensors determined for hCc in this and earlier works. $\Delta\chi_{ax}$ and $\Delta\chi_{rh}$ are the axial and rhombic components of the $\Delta\chi$ tensor in units of 10^{-32} m^3 ; β and κ are the angles (in degrees) relating the $\Delta\chi$ -tensor frame to the molecular coordinate system (Fig. 3b)

$\Delta\chi_{ax}$	$\Delta\chi_{rh}$	β	κ	Reference
3.10 ± 0.05	1.50 ± 0.13	11 ± 1	9 ± 2	This work ^a
2.87 ± 0.45	1.11 ± 0.29	15 ± 5	6 ± 8	This work ^b
3.43	1.23	13	3	(Liu et al. 2003) ^a
3.35	1.36	13	3	(Liu et al. 2003) ^{a,c}
2.72 ± 0.26	1.44 ± 0.14	18	12	(Banci et al. 1997b) ^a
2.68 ± 0.1	1.25 ± 0.12	7	10	(Banci et al. 1997b) ^d
2.29	1.7	15	11	(Qi et al. 1996) ^e
3.01	1.34	15	8	(Turner and Williams 1993) ^a
3.43	1.1	13	3	(Feng et al. 1990) ^a

For details see Table S2 and the “Experimental section”

^a The X-ray structure of hCc^{ox} was used in the calculations; ^b The reported values are the averages of $\Delta\chi$ parameters obtained from five hCc structures (Table S2); the errors are standard deviations; ^c The values are for the H26 N/H33 N hCc; ^d The NMR structure of hCc^{ox} (PDB ID 1AKK) was used as an input; ^e The NMR structure of hCc^{ox} (PDB ID 1OCD) was used in the calculations

are in good agreement with the parameters calculated for tuna Cc ($\Delta\chi_{ax} = 3.40$, $\Delta\chi_{rh} = 1.48$, $\beta = 13.5$, $\kappa = 9.5$; Feng et al. 1990). This finding suggests that the magnitude and the orientation of the $\Delta\chi$ tensors are conserved among the eukaryotic cytochromes, a family of proteins with a high degree of sequence and structure conservation (Banci and Assfalg 2001).

The correlation plots of the experimental $\Delta\delta_{obs}$ versus PCSs back-calculated from the determined $\Delta\chi$ tensors (δ_{PCS}^{cal}) are shown in Fig. 4 (yCc) and Fig. S3 (hCc). Backbone ^1H , ^{13}C , and ^{15}N atoms exhibit good correlations, with most of the points lying close to the diagonal. As reported before (Boyd et al. 1999), the N nuclei show the highest variance, due to their high sensitivity to small changes in the chemical environment. For the residues not in direct contact with the haem, the $\Delta\delta_{obs}$ is exactly equal to (δ_{PCS}^{cal}) (2), providing that the structures of the reduced

and oxidized protein are the same. However, the correlations plots for yCc and hCc contain a number of outliers (Figs. 4 and S3) indicating that both cytochromes undergo redox-dependent structural changes.

Redox-dependent changes

As can be seen from Fig. 5a–e, where the difference between $\Delta\delta_{obs}$ and (δ_{PCS}^{cal}) for various nuclei is plotted against the residue number, several contiguous stretches of yCc exhibit large deviations (highlighted regions in Fig. 5). In this work it is assumed that the unpaired electron is centred on the iron atom, while in fact it is distributed over the conjugated π -system of the haem, which can introduce discrepancies between $\Delta\delta_{obs}$ and δ_{PCS}^{cal} values for protein atoms in the vicinity of the prosthetic group. However, $|\Delta\delta_{obs} - \delta_{PCS}^{cal}|$ terms for yCc nuclei do not correlate with

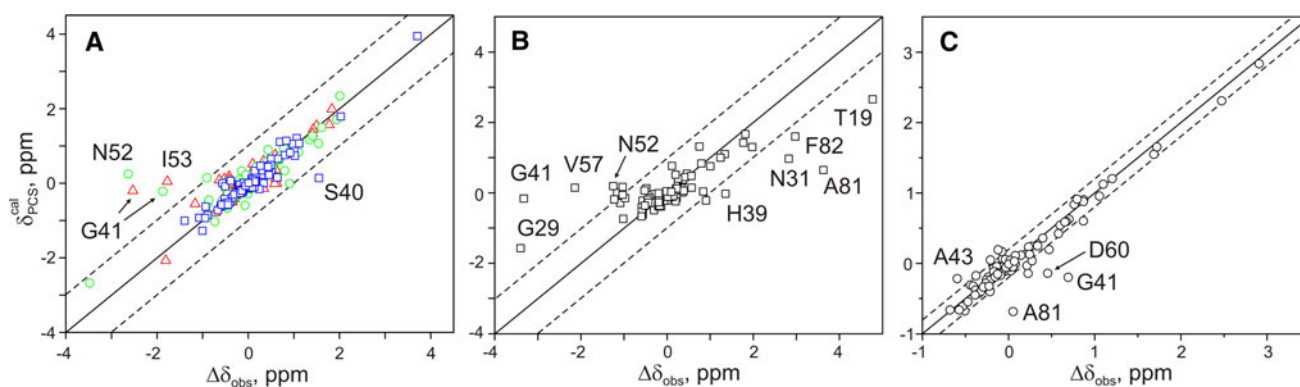


Fig. 4 Comparison of the differences in chemical shifts between the oxidized and reduced yCc ($\Delta\delta_{obs}$) and calculated PCSs (δ_{PCS}^{cal}). The latter values were obtained for **a** CO (red triangles), C_α (green circles), C_β (blue squares); **b** N; and **c** HN atoms from the X-ray

structure of yCc^{red} and the corresponding $\Delta\chi$ tensor determined in this study. Dashed lines indicate cut-offs used in the $\Delta\chi$ tensor fitting (see “Experimental section”). The most prominent outliers are indicated by the labels

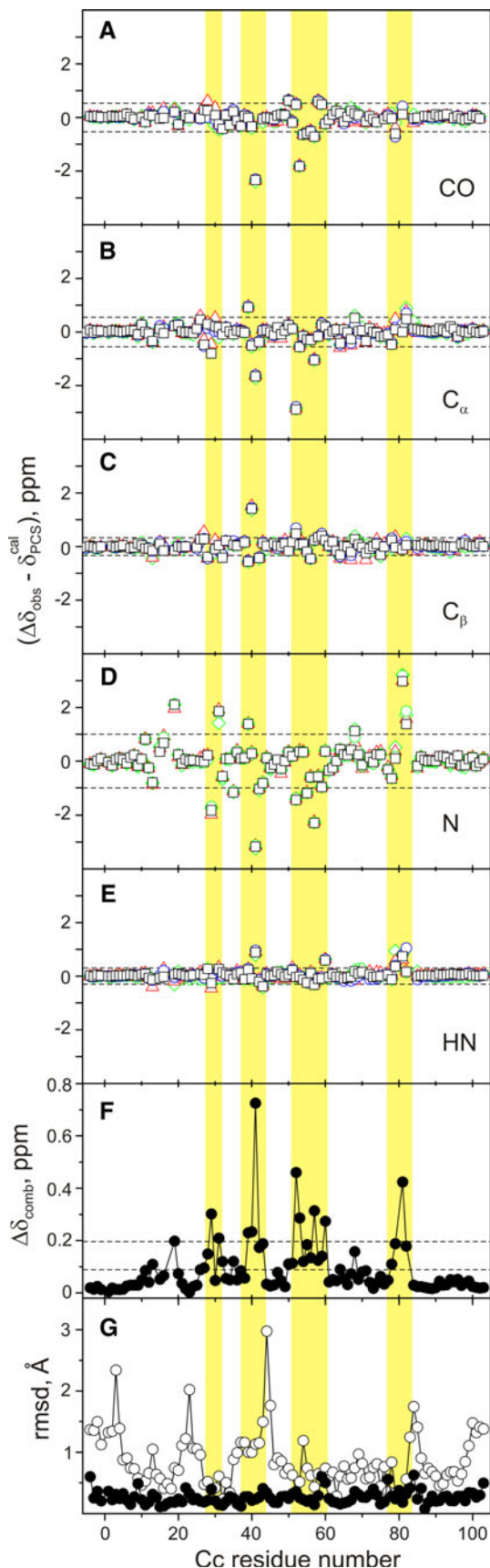


Fig. 5 Distribution of yCc residues involved in redox-dependent changes as determined by paramagnetic NMR spectroscopy (this work, **a–f**) and conventional structural analyses (previous studies, **g**). (**a–e**) Distribution of $(\Delta\delta_{\text{obs}} - \delta_{\text{PCS}}^{\text{cal}})$ terms for **a** CO, **b** C_{α} , **c** C_{β} , **d** N, and **e** HN atoms as a function of yCc residue number. Dashed lines denote the average plus one standard deviation calculated over all atoms in a given category. $\delta_{\text{PCS}}^{\text{cal}}$ values were computed from the X-ray (blue circles—yCc^{ox}; black squares—yCc^{red}) and NMR (green diamonds—yCc^{ox}; red triangles—yCc^{red}) structures using the $\Delta\chi$ tensor determined in this work. **f** The combined, per-residue difference between $\Delta\delta_{\text{obs}}$ and $\delta_{\text{PCS}}^{\text{cal}}$, $\Delta\delta_{\text{comb}}$, as defined in (7). Dashed lines denote the average and the average plus one standard deviation. Stretches of residues exhibiting redox-dependent changes are highlighted. **g** Pairwise backbone root-mean-square deviations between the structures of the reduced and oxidized yCc as determined by X-ray (filled symbols) and NMR (open symbols)

the distances to the haem iron, signifying that the detected differences are not due to simplifications inherent to the computational model. Moreover, multiple atoms of the same residue exhibit $|\Delta\delta_{\text{obs}} - \delta_{\text{PCS}}^{\text{cal}}| > 0$, reinforcing the conclusion that the observed discrepancies are not caused by random experimental errors, but rather report on the redox-dependent Cc behaviour in solution. When $(\Delta\delta_{\text{obs}} - \delta_{\text{PCS}}^{\text{cal}})$ terms for various nuclei are combined into single, per-residue values ($\Delta\delta_{\text{comb}}$, (7)), it appears that yCc residues 28–31, 39–43, 52–60, and 79–82 show significant differences between $\Delta\delta_{\text{obs}}$ and $\delta_{\text{PCS}}^{\text{cal}}$ (Fig. 5f), regardless of the structure used for $\delta_{\text{PCS}}^{\text{cal}}$ calculation (different symbols in Fig. 5a–e). Residues 41, 52, and 81 show the largest $\Delta\delta_{\text{comb}}$ values (Fig. 5f), while no effects are observed for N- and C-terminal α -helices—the most stable secondary structure elements of Cc.

The affected areas map out onto a single patch on yCc, surrounding the haem propionate 7 (Pr7) and comprising the loop harbouring the M80 ligand to the iron (Fig. 6). As seen in Cc X-ray structures (Berghuis and Brayer 1992; Louie and Brayer 1990), residues G41 and N52 are part of a hydrogen-bond network involving Pr7. Moreover, studies of yCc in solution by nuclear Overhauser enhancement (NOE) spectroscopy reported a conformational change of Pr7 group and a concomitant re-orientation of the N52 side-chain upon Cc reduction (Baistrocchi et al. 1996; Banci et al. 1997a). These findings suggest that the redox-dependent structural changes detected by paramagnetic NMR in this work likely involve re-organization of the H-bond network around Pr7 and the adjacent loop bearing the M80 group. Despite this agreement, the areas with high $\Delta\delta_{\text{comb}}$ do not coincide with protein regions showing high root-mean-square deviations (rmsd) between backbone atoms in the reduced and oxidized structures determined by X-ray crystallography or conventional, NOE-based NMR spectroscopy (Fig. 5g). A possible explanation for this finding is that chemical shifts, which form the basis of the PCS analysis performed in this work, are sensitive to subtle changes in the chemical environment of the observed

nuclei, rather than their absolute positions in the molecular reference frame.

The distribution of $(\Delta\delta_{\text{obs}} - \delta_{\text{PCS}}^{\text{cal}})$ terms in hCc sequence (Fig. S4) is very similar to that of yCc, with $\Delta\delta_{\text{comb}}$ values peaking in the same regions. Given the large differences among the reported crystallographic and NMR structures of hCc, the numerical values of $\Delta\delta_{\text{comb}}$ depend on the structure used in the $\delta_{\text{PCS}}^{\text{cal}}$ calculations (different symbols in Fig. S4a–e), yet qualitatively the affected regions remain the same. As in the case of yCc, the areas with high $\Delta\delta_{\text{comb}}$ do not coincide with protein regions showing high backbone rmsd between hCc^{ox} and hCc^{red} coordinates (Fig. S4g). These findings indicate that both yCc and hCc undergo very similar redox-dependent structural changes, the extent of which is likely conserved in the protein family.

Providing that the experimental conditions of the reduced and oxidized protein samples closely match, the $(\Delta\delta_{\text{obs}} - \delta_{\text{PCS}}^{\text{cal}})$ term is a measure of the diamagnetic chemical shift differences arising from redox-dependent structural changes, i.e. $(\Delta\delta_{\text{obs}} - \delta_{\text{PCS}}^{\text{cal}}) \approx \Delta\delta_{\text{struct}}$ [from (2)]. In order to assess whether the differences between the

experimental structures of the oxidized and reduced yCc could give rise to the observed $(\Delta\delta_{\text{obs}} - \delta_{\text{PCS}}^{\text{cal}})$ terms, we have predicted diamagnetic chemical shifts of yCc^{ox} and yCc^{red} (Fig. S5). For yCc in both redox states, there is a good correlation between the experimentally measured (δ_{obs}) and calculated (δ_{cal}) diamagnetic chemical shifts for C_α and C_β atoms. For CO, N, and HN nuclei, the predictions are highly imprecise and, thus, were excluded from further analysis. For all atoms, the δ_{cal} values derived from the X-ray coordinates correlate better with δ_{obs} than those obtained from the NMR structures (Fig. S5). The average deviations between δ_{obs} and δ_{cal} , determined for C_α and C_β atoms in the X-ray structures, are $|\delta_{\text{obs}} - \delta_{\text{cal}}| = 0.89 \pm 0.67$ ppm and 0.83 ± 0.64 ppm for yCc^{ox} and yCc^{red}, respectively. The difference between the δ_{cal} values in the oxidized and reduced forms provides an estimate of the diamagnetic chemical shift changes in a given pair of

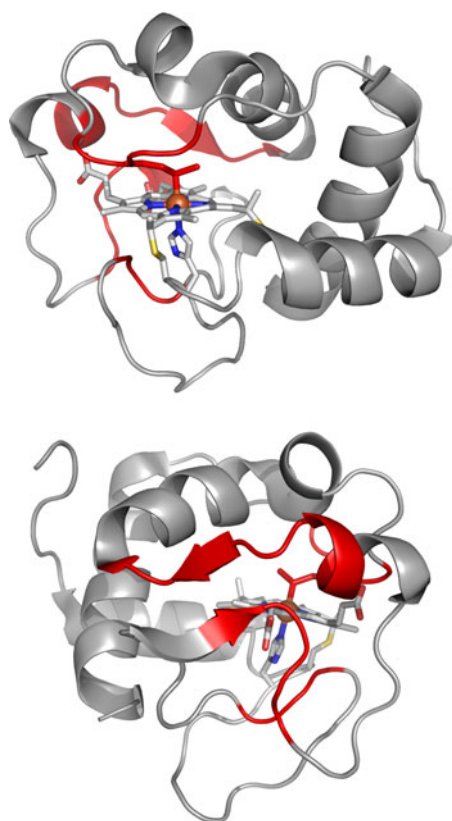


Fig. 6 Location of yCc residues experiencing redox-dependent structural changes. The residues with large discrepancies between $\Delta\delta_{\text{obs}}$ and $\delta_{\text{PCS}}^{\text{cal}}$ are coloured red. The front and back views of yCc are shown. The protein orientation in the upper panel is the same as in Fig. 3a. See the legend to Fig. 3a for more details

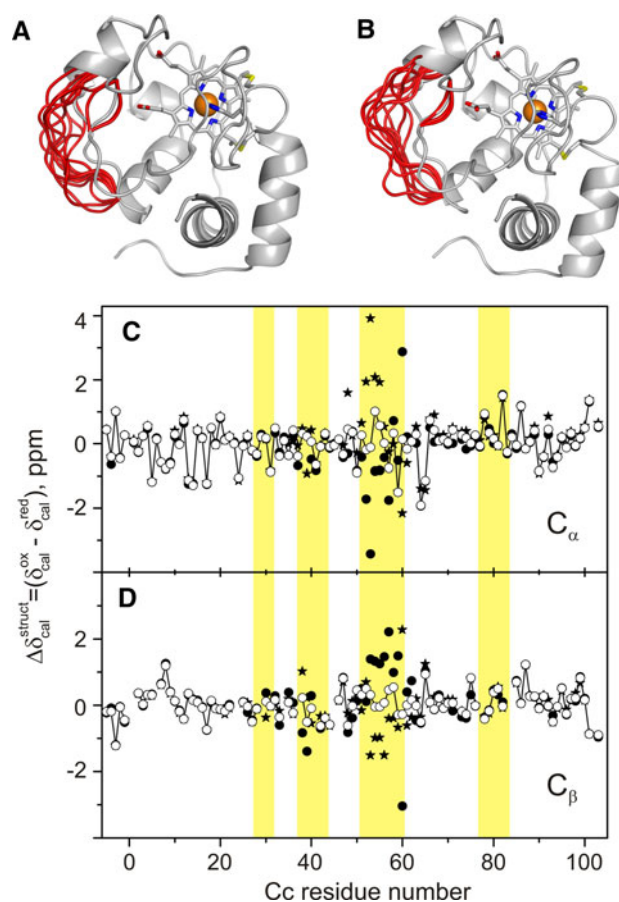


Fig. 7 Simulated mobility of the yCc regions involved in redox-dependent structural changes. **a–b** X-ray structures of **a** yCc^{red} and **b** yCc^{ox} with 10 best solutions for the randomized regions (*red cartoons*). **c–d** Differences between the chemical shifts for **c** C_α and **d** C_β nuclei in the reduced and oxidized proteins calculated from: the corresponding X-ray structures (*open circles*); the simulated ensemble of yCc^{red} and the X-ray structure of yCc^{ox} (*filled stars*); and the X-ray structure of yCc^{red} and the simulated ensemble of yCc^{ox} (*filled circles*). Highlighted regions are the same as in Fig. 5

Table 4 Cc structures used in this study

Cc	Method	State	PDB ID	Reference
yCc	Xray	ox	2YCC	(Berghuis and Brayer 1992)
		red	1YCC	(Louie and Brayer 1990)
	NMR	ox	1YIC	(Banci et al. 1997a)
		red	1YFC	(Baistrocchi et al. 1996)
hCc	Xray	ox	1HRC	(Bushnell et al. 1990)
	NMR, Banci et al.	ox	1AKK	(Banci et al. 1997b)
		red	1GIW	(Banci et al. 1999a)
	NMR, Wand and co-workers	ox	1OCD	(Qi et al. 1996)
		red	2FRC	(Qi et al. 1996)

yCc^{ox} and yCc^{red} structures ($\Delta\delta_{\text{cal}}^{\text{struct}} = \delta_{\text{cal}}^{\text{ox}} - \delta_{\text{cal}}^{\text{red}}$). For the crystallographic coordinates, the plots of $\Delta\delta_{\text{cal}}^{\text{struct}}$ versus residue number exhibit nearly flat profiles (open circles in Fig. 7c–d), with no extra features in the regions showing large deviations in Fig. 5b–c. A similar picture is obtained for the $\Delta\delta_{\text{cal}}^{\text{struct}}$ calculated from the NMR structures (data not shown). Notwithstanding large errors on the predicted δ_{cal} values, these findings indicate that the differences between the experimental structures of the oxidized and reduced yCc cannot account for the observed discrepancies between $\Delta\delta_{\text{obs}}$ and $\delta_{\text{PCS}}^{\text{cal}}$.

Although detailed analysis of possible redox-dependent structural changes is outside the scope of this work, we have attempted to simulate the mobility of the affected Cc regions and assess whether protein dynamics could account for the profiles in Fig. 5b–c. Starting from the X-ray coordinates of yCc, we generated ensembles of protein structures, where residues 39–41 and 52–60 were given torsional freedom, while the rest of the protein was fixed (see [Experimental section](#)). Note that we did not model the mobility of Cc residues 79–82 (lying in one the regions showing deviations in Fig. 5a–f and bearing the M80 ligand to the haem group) in order to preserve the haem ligation geometry. The resulting ensembles of 10 best solutions for yCc in both oxidation states are shown in Fig. 7a–b. The atoms in the modelled regions experience only small changes in PCSs relative to those in the X-ray structures, with the deviations ranging from –0.15 to 0.19 ppm for C, C_α, C_β, N, and HN nuclei. However, the ensemble-averaged diamagnetic chemical shifts, obtained from the δ_{calc} values calculated for C_α and C_β atoms in each of the 10 solutions, exhibit large differences with those derived from the X-ray structures (Fig. 7c–d). The values of $\Delta\delta_{\text{cal}}^{\text{struct}}$ calculated from the yCc^{red} simulated ensemble and the yCc^{ox} X-ray structure (stars, Fig. 7c–d) are of opposite sign to those derived from the yCc^{ox} ensemble and the yCc^{red} crystallographic coordinates (filled circles, Fig. 7c–d), yet the two patterns are very similar. Although the absolute values of the ensemble-based $\Delta\delta_{\text{cal}}^{\text{struct}}$

(Fig. 7c–d) and experimentally-determined $\Delta\delta_{\text{struct}} \approx (\Delta\delta_{\text{obs}} - \delta_{\text{PCS}}^{\text{cal}})$ (Fig. 5b–c) for the residues in the modelled regions do not match, the sign of $\Delta\delta_{\text{cal}}^{\text{struct}}$ derived from the latter dataset agrees with that of $\Delta\delta_{\text{struct}}$. This finding suggests that elevated mobility of Cc loop regions in the oxidized state could give rise to the observed $(\Delta\delta_{\text{obs}} - \delta_{\text{PCS}}^{\text{cal}})$ profiles (Fig. 5a–f). It should be noted that the modelling procedure used in this work provides only a rough picture of the extent of motional freedom available to the Cc regions in question, which—together with high errors on the predicted diamagnetic chemical shifts—could explain the large discrepancies between $\Delta\delta_{\text{cal}}^{\text{struct}}$ and $\Delta\delta_{\text{struct}}$ values. Further efforts will definitely be required to obtain a more accurate description of the redox-dependent changes in Cc dynamics in solution.

Comparison with previous studies

The approach to assess redox-dependent changes in Cc structure from paramagnetic shifts was pioneered by Williams et al. (1985) and later used for the cytochromes from tuna (Williams et al. 1985), horse (Feng et al. 1990; Turner and Williams 1993), yeast (Boyd et al. 1999; Gao et al. 1991), and Cc-551 from *Pseudomonas aeruginosa* (Timkovich and Cai 1993). In most cases, a set of assigned proton resonances and an X-ray structure of Cc available at a time served as a basis for the $\Delta\chi$ tensor determination and subsequent comparison of the back-calculated and measured PCS values. The general consensus from the previous studies is that the structure of Cc is largely the same in both oxidation states. However, except for the work on Cc-551 from *P. aeruginosa*, which found no discrepancies between $\Delta\delta_{\text{obs}}$ and $\delta_{\text{PCS}}^{\text{cal}}$ values (Timkovich and Cai 1993), all studies reported significant $(\Delta\delta_{\text{obs}} - \delta_{\text{PCS}}^{\text{cal}})$ terms for a number of residues. The presence of large deviations in 39–42 and 48–59 regions of hCc (Feng et al. 1990), later confirmed by ¹H and ¹³C PCSs analysis (Turner and Williams 1993), allowed the authors to postulate that “[the

redox-dependent] change runs on M80 side of the haem and involves hydrogen-bond network including Trp59, the haem propionates, Gly41 and at least two water molecules” (Williams et al. 1985). Similarly, large discrepancies for the yCc residues 38–43, 51–52, and 60–71 (Gao et al. 1991), most of which were later corroborated by PCS analysis of ^{15}N backbone amide atoms (Boyd et al. 1999), were interpreted as an evidence for redox-dependent structural changes. Our findings agree best with those of Feng et al. (Feng et al. 1990), whose outline of the protein region experiencing differences in the oxidized and reduced states closely matches the one determined here.

The differences between the oxidized and reduced Cc were further investigated by HD exchange spectroscopy (Banci et al. 1997a; Baxter and Fetrow 1999). In the work of Banci et al. most of the differences in the HD behavior were found to involve residues 14–26 and 75–82 (Banci et al. 1997a), while Baxter and Fetrow reported that the observed differences are interspersed around all structural elements of the protein (Baxter and Fetrow 1999). Despite this disagreement, both studies have concurred that Cc^{ox} appears to be more flexible than Cc^{red} , a conclusion which was later confirmed by an NMR relaxation analysis (Fetrow and Baxter 1999).

Conclusions

In this work, we have re-assessed the differences between reduced and oxidized Cc in solution using an extensive experimental dataset comprising over 450 measured PCSs and high-resolution X-ray and solution NMR structures of yCc and hCc. We find that, in both proteins, the region clustered around G41, N52, and A81 residues consistently exhibits significant differences between the observed and calculated PCSs, indicative of redox-dependent structural changes. It is not clear whether these rearrangements play a role in the modulation of the electron transfer between Cc and its binding partners, a question that has prompted a lasting debate (Banci et al. 2000). We suggest that the observed discrepancies arise from redox-dependent changes in protein dynamics, possibly mediated by re-organization of H-bond network involving Pr7 and the M80-bearing loop, rather than gross structural perturbations. The higher flexibility of Cc in the oxidized than reduced form might have clear functional implications, such as enhancing dissociation from the protein complex once the electron transfer is complete. Such modulation of protein function by change in dynamics, observed by paramagnetic NMR spectroscopy in solution, could represent a case of “subtle allostery” in a small, single-domain protein, with little room for large conformational changes conventionally associated with the allosteric regulation.

Experimental section

Sample preparation

The pUCcc plasmid carrying the gene coding for the T-5A/C102T yCc variant studied in this work was provided by Dr. Jonathan Worrall (University of Essex, United Kingdom). The expression vector for the wt hCc was derived from the pJRhrsN2 construct (Rumbley et al. 2002) coding for the H26N/H33N hCc (provided by Dr. Marcellus Ubbink of Leiden University, the Netherlands). The H26N and H33N mutations were reverted in two sequential site-directed mutagenesis steps using whole plasmid synthesis polymerase chain reaction protocol (Weiner et al. 1994). The proteins were expressed in *Escherichia coli* using a published procedure (Pollock et al. 1998), employing co-expression of the genes encoding for the Cc and the Cc haem lyase, the protein required for the haem insertion. Uniformly-labelled ^{15}N and [^{13}C , ^{15}N] cytochromes were produced in the M9 minimal medium (Morar et al. 1999) containing $^{15}\text{NH}_4\text{Cl}$ and $^{13}\text{C}_6$ -glucose as the sole nitrogen and carbon sources, respectively, and supplemented with δ -aminolevulinic acid, the first committed precursor of the haem biosynthesis. Both yCc and hCc were purified as described elsewhere (Morar et al. 1999; Pollock et al. 1998), with size-exclusion chromatography as an additional purification step. Once purified, the proteins were oxidized with an excess of $\text{K}_3[\text{Fe}(\text{CN})_6]$, exchanged into an NMR buffer, concentrated to 1–2 mM, and stored at -20°C until required. The protein concentrations and purity were estimated from UV–vis spectra using, respectively, the extinction coefficient $\epsilon_{410} = 106.1 \text{ mM}^{-1} \text{ cm}^{-1}$ and the absorbance peak ratio of $A_{410}/A_{280} \geq 4.0$. Cc^{red} was prepared by the addition of a twofold molar excess of sodium ascorbate to the Cc^{ox} samples. All NMR samples contained 1 mM Cc in 20 mM sodium phosphate pH 6.0 (containing 0.1 M NaCl for the high-salt datasets) and 6% D_2O for the lock.

NMR spectroscopy

All experiments were performed at 303 K on Varian NMR Direct-Drive Systems 600 and 800 MHz spectrometers, the latter equipped with a salt tolerance triple-resonance PFG-Z cold probe. For the high-salt samples, a set of 2D [^1H , ^{15}N] HSQC and 3D HNCACB, CBCA(CO)NH, and HNCO spectra was acquired on U- ^{13}C , ^{15}N] proteins. For the U- ^{15}N proteins at low salt, 2D [^1H , ^{15}N] HSQC and 3D ^{15}N -edited NOESY-HSQC (100 ms mixing time) spectra were recorded. All NMR data were processed in NMRPipe (Delaglio et al. 1995) and analysed in CCPN (Vranken et al. 2005). For the high-salt samples, sequential backbone assignments were obtained by connecting $^{13}\text{C}_\alpha$ and $^{13}\text{C}_\beta$

frequencies from the HNCACB and CBCA(CO)NH spectra at the ^1H , ^{15}N frequencies of every peak in the [^1H , ^{15}N] HSQC spectrum. Subsequently, ^{13}C resonances were assigned from the HNCO spectrum at the assigned ^1H , ^{15}N frequencies. Finally, the heavy-atom side-chain resonances of Asn and Gln residues were assigned from CBCA(-CO)NH and HNCO spectra by connecting the ^1H , ^{15}N side-chain amide resonances to the corresponding C_α and C_β frequencies. The assignments of 2D [^1H , ^{15}N] HSQC resonances obtained at 0.1 M NaCl were transferred to the low-salt datasets and verified by 3D ^{15}N -edited NOESY-HSQC experiments. The assignments determined in this work were deposited in the BMRB data bank under accession numbers 17,845 (yCc^{ox}), 17,846 (yCc^{red}), 17,847 (hCc^{ox}), and 17,848 (hCc^{red}).

Paramagnetic NMR analysis

The dipolar pseudocontact shift (δ_{PCS}) is given by (3) (Ubbink et al. 2002):

$$\delta_{\text{PCS}} = \frac{1}{12\pi} r^{-3} [\Delta\chi_{\text{ax}}(3 \cos^2 \theta - 1) + 3/2 \Delta\chi_{\text{rh}} \sin^2 \theta \cos^2 \phi] \quad (3)$$

where r , θ , and ϕ are the polar coordinates of the nuclear spin with respect to the principal axes of the magnetic susceptibility tensor ($\Delta\chi$), and $\Delta\chi_{\text{ax}}$ and $\Delta\chi_{\text{rh}}$ are, respectively, the axial and rhombic components of the $\Delta\chi$ tensor defined as:

$$\Delta\chi_{\text{ax}} = \chi_{zz} - 1/2(\chi_{xx} - \chi_{yy}) \quad (4)$$

$$\Delta\chi_{\text{rh}} = \chi_{xx} - \chi_{yy}, \quad (5)$$

where χ_{xx} , χ_{yy} , and χ_{zz} are the principal components of the χ tensor. In the absence of the zero-field splitting, the relationship between χ - and g -tensors is given by (6) (Bertini et al. 2002):

$$\chi_{kk} = \mu_0 \mu_{\text{B}}^2 g_{kk}^2 \frac{S(S+1)}{3kT} \quad (6)$$

where $k = (x, y, \text{ or } z)$, μ_0 is the permeability of vacuum, μ_{B} is the electron Bohr magneton, S is the electron spin number, k is the Boltzmann constant, and T is the temperature. We used (6) to convert the g -tensors, sometimes reported in the literature, to the χ tensors used here. Throughout this work, we report the $\Delta\chi$ values in 10^{-32} m^3 units and follow the “ZYZ” convention for the Euler angles as implemented in Numbat software (Schmitz et al. 2008).

The $\Delta\chi$ tensors were calculated with Numbat (Schmitz et al. 2008), starting from a set of measured $\Delta\delta_{\text{obs}}$ values (Tables S1 and S2) and protein structures (Table 4). The residues in direct contact with the haem group (C14, C17, H18, and M80) and, thus, with a non-negligible contact

shift contribution to $\Delta\delta_{\text{obs}}$, were excluded from the analysis throughout this work. Atoms with $|\Delta\delta_{\text{obs}} - \delta_{\text{PCS}}^{\text{cal}}| > 1$ ppm (for ^{13}C and ^{15}N nuclei) or > 0.2 ppm (for protons) were excluded from the dataset during iterative refinement of the $\Delta\chi$ tensors. The calculated tensors were corrected for the residual anisotropic chemical shifts (RACS; John et al. 2005) using RACS correction term implemented in Numbat (Schmitz et al. 2008). The errors on the $\Delta\chi$ parameters were estimated with a Monte-Carlo protocol (Schmitz et al. 2008) by adding 10% of Gaussian noise to the atomic coordinates and experimental $\Delta\delta_{\text{obs}}$ values and randomly excluding 10% of the working PCS dataset.

The combined, per-residue difference between $\Delta\delta_{\text{obs}}$ and $\delta_{\text{PCS}}^{\text{cal}}$ is given by (7):

$$\Delta\delta_{\text{comb}} = \sqrt{\frac{\sum_i \Delta\delta_i^2}{n}} \quad (7)$$

where $\Delta\delta_i = (\Delta\delta_{\text{obs},i} - \delta_{\text{PCS},i}^{\text{cal}})/m$, with $m = 1, 3, 5$ for ^1H , ^{13}C , and ^{15}N nuclei, respectively; summation is carried over all atoms with the measured ($\Delta\delta_{\text{obs}} - \delta_{\text{PCS}}^{\text{cal}}$) term; n is the number of such atoms.

Diamagnetic chemical shift calculations and Cc modelling

Chemical shifts at pH 6.0 and 303 K were predicted from yCc structures with ShiftX2 (Han et al. 2011). The yCc conformational ensembles were generated in Xplor-NIH (Schwieters et al. 2003) by simulated annealing in torsion angle space with standard protein geometry and vdW parameters and knowledge-based dihedral angle potentials (Iwahara et al. 2004). The coordinates of yCc^{ox} and yCc^{red} were taken from the respective crystal structures (Table 4). Residues 39–41 and 52–60 were given full torsional freedom, protein sidechains within 5 Å of the modelled regions were allowed to move, while the rest of the protein (including the haem group and its ligands C14, C17, H18, and M80) was kept fixed. In a typical run, 100 structures were output, ranked by the total energy, and 10 best selected for further analysis.

Acknowledgments We thank Dr. Jonathan Worrall and Prof. Marcellus Ubbink for the kind gifts of the Cc expression vectors, Dr. Christophe Schmitz for useful tips on the installation and use of Numbat software, and Dr. Lieven Buts for the help with the data analysis. ANV is an FWO Post-Doctoral Researcher.

References

- Baistrocchi P, Banci L, Bertini I, Turano P, Bren KL, Gray HB (1996) Three-dimensional solution structure of *Saccharomyces cerevisiae* reduced *iso*-1-cytochrome *c*. *Biochemistry* 35:13788–13796

- Banci L, Assfalg M (2001) Mitochondrial cytochrome *c*. In: Messerschmidt A, Huber R, Poulos TL, Wieghardt K (eds) Handbook of metalloproteins. Wiley, Chichester, pp 33–43
- Banci L, Bertini I, Bren KL, Gray HB, Sompornpisut P, Turano P (1997a) Solution structure of oxidized *Saccharomyces cerevisiae* *iso*-1-cytochrome *c*. *Biochemistry* 36:8992–9001
- Banci L, Bertini I, Gray HB, Luchinat C, Reddig T, Rosato A, Turano P (1997b) Solution structure of oxidized horse heart cytochrome *c*. *Biochemistry* 36:9867–9877
- Banci L, Bertini I, Huber JG, Spyroulias GA, Turano P (1999a) Solution structure of reduced horse heart cytochrome *c*. *J Biol Inorg Chem* 4:21–31
- Banci L, Bertini I, Rosato A, Varani G (1999b) Mitochondrial cytochromes *c*: a comparative analysis. *J Biol Inorg Chem* 4: 824–837
- Banci L, Bertini I, Luchinat C, Turano P (2000) Solution structures of hemoproteins. In: Kadish KM, Smith KM, Guilard R (eds) The porphyrin handbook. Academic Press, San Diego, CA, pp 323–350
- Baxter SM, Fetow JS (1999) Hydrogen exchange behavior of [U - ^{15}N]-labeled oxidized and reduced *iso*-1-cytochrome *c*. *Biochemistry* 38:4493–4503
- Berghuis AM, Brayer GD (1992) Oxidation state-dependent conformational changes in cytochrome *c*. *J Mol Biol* 223:959–976
- Bertini I, Luchinat C, Parigi G (2002) Magnetic susceptibility in paramagnetic NMR. *Progress in Nuclear Magnetic Resonance Spectroscopy* 40:249–273
- Boyd J, Dobson CM, Morar AS, Williams RJP, Pielak GJ (1999) ^1H and ^{15}N hyperfine shifts of cytochrome *c*. *J Am Chem Soc* 121:9247–9248
- Bushnell GW, Louie GV, Brayer GD (1990) High-resolution three-dimensional structure of horse heart cytochrome *c*. *J Mol Biol* 214:585–595
- Delaglio F, Grzesiek S, Vuister GW, Zhu G, Pfeifer J, Bax A (1995) NMRPipe: a multidimensional spectral processing system based on UNIX pipes. *J Biomol NMR* 6:277–293
- DeLano WL (2002) The PyMOL molecular graphics system. DeLano Scientific, Palo Alto
- Feng YQ, Roder H, Englander SW (1990) Redox-dependent structure change and hyperfine nuclear magnetic resonance shifts in cytochrome *c*. *Biochemistry* 29:3494–3504
- Fetow JS, Baxter SM (1999) Assignment of ^{15}N chemical shifts and ^{15}N relaxation measurements for oxidized and reduced *iso*-1-cytochrome *c*. *Biochemistry* 38:4480–4492
- Gao Y, Boyd J, Williams RJP, Pielak GJ (1990) Assignment of proton resonances, identification of secondary structural elements, and analysis of backbone chemical shifts for the C102T variant of yeast *iso*-1-cytochrome *c* and horse cytochrome *c*. *Biochemistry* 29:6994–7003
- Gao Y, Boyd J, Pielak GJ, Williams RJP (1991) Comparison of reduced and oxidized yeast *iso*-1-cytochrome *c* using proton paramagnetic shifts. *Biochemistry* 30:1928–1934
- Han B, Liu Y, Ginzinger S, Wishart D (2011) SHIFTX2: significantly improved protein chemical shift prediction. *J Biomol NMR* 50:43–57
- Iwahara J, Schwieters CD, Clore GM (2004) Ensemble approach for NMR structure refinement against ^1H paramagnetic relaxation enhancement data arising from a flexible paramagnetic group attached to a macromolecule. *J Am Chem Soc* 126:5879–5896
- John M, Park AY, Pintacuda G, Dixon NE, Otting G (2005) Weak alignment of paramagnetic proteins warrants correction for residual CSA effects in measurements of pseudocontact shifts. *J Am Chem Soc* 127:17190–17191
- Levitt M, Perutz MF (1988) Aromatic rings act as hydrogen bond acceptors. *J Mol Biol* 201:751–754
- Liu W, Rumbley J, Englander SW, Wand AJ (2003) Backbone and side-chain heteronuclear resonance assignments and hyperfine NMR shifts in horse cytochrome *c*. *Prot Sci* 12:2104–2108
- Louie GV, Brayer GD (1990) High-resolution refinement of yeast *iso*-1-cytochrome *c* and comparisons with other eukaryotic cytochromes *c*. *J Mol Biol* 214:527–555
- Moench SJ, Shi TM, Satterlee JD (1991) Proton-NMR studies of the effects of ionic strength and pH on the hyperfine-shifted resonances and phenylalanine-82 environment of three species of mitochondrial ferricytochrome *c*. *Eur J Biochem* 197:631–641
- Morar AS, Kakouras D, Young GB, Boyd J, Pielak GJ (1999) Expression of ^{15}N -labeled eukaryotic cytochrome *c* in *Escherichia coli*. *J Biol Inorg Chem* 4:220–222
- Pollock WBR, Rosell FI, Twitchett MB, Dumont ME, Mauk AG (1998) Bacterial expression of a mitochondrial cytochrome *c*. Trimethylation of Lys 72 in yeast *iso*-1-cytochrome *c* and the alkaline conformational transition. *Biochemistry* 37:6124–6131
- Qi PX, Beckman RA, Wand AJ (1996) Solution structure of horse heart ferricytochrome *c* and detection of redox-related structural changes by high-resolution ^1H NMR. *Biochemistry* 35: 12275–12286
- Rule GS, Hitchens TK (2006) Fundamentals of protein NMR spectroscopy. Springer, Dordrecht
- Rumbley JN, Hoang L, Englander SW (2002) Recombinant equine cytochrome *c* in *Escherichia coli*: high-level expression, characterization, and folding and assembly mutants. *Biochemistry* 41:13894–13901
- Schmitz C, Stanton-Cook MJ, Su X-C, Otting G, Huber T (2008) Numbat: an interactive software tool for fitting $\Delta\chi$ -tensors to molecular coordinates using pseudocontact shifts. *J Biomol NMR* 41:179–189
- Schwieters CD, Kuszewski JJ, Tjandra N, Clore GM (2003) The Xplor-NIH NMR molecular structure determination package. *J Magn Reson* 160:66–74
- Sukits SF, Erman JE, Satterlee JD (1997) Proton NMR assignments and magnetic axes orientations for wild-type yeast *iso*-1-ferricytochrome *c* free in solution and bound to cytochrome *c* peroxidase. *Biochemistry* 36:5251–5259
- Timkovich R, Cai M (1993) Investigation of the structure of oxidized *Pseudomonas aeruginosa* cytochrome *c*-551 by NMR: comparison of observed paramagnetic shifts and calculated pseudocontact shifts. *Biochemistry* 32:11516–11523
- Turner DL, Williams RJP (1993) ^1H and ^{13}C NMR investigation of redox-state-dependent and temperature-dependent conformational changes in horse cytochrome *c*. *Eur J Biochem* 211:555–562
- Ubbink M, Worrall JAR, Canters GW, Groenen EJJ, Huber M (2002) Paramagnetic resonance of biological metal centers. *Ann Rev Biophys Biomol Struct* 31:393–422
- Vranken WF, Boucher W, Stevens TJ, Fogh RH, Pajon A, Llinas M, Ulrich EL, Markley JL, Ionides J, Laue ED (2005) The CCPN data model for NMR spectroscopy: development of a software pipeline. *Proteins* 59:687–696
- Weiner MP, Costa GL, Schoettlin W, Cline J, Mathur E, Bauer JC (1994) Site-directed mutagenesis of double-stranded DNA by the polymerase chain reaction. *Gene* 151:119–123
- Williams G, Clayden NJ, Moore GR, Williams RJP (1985) Comparison of the solution and crystal structures of mitochondrial cytochrome *c*—analysis of paramagnetic shifts in the nuclear magnetic resonance spectrum of ferricytochrome *c*. *J Mol Biol* 183:447–460
- Worrall JAR, Kolczak U, Canters GW, Ubbink M (2001) Interaction of yeast *iso*-1-cytochrome *c* with cytochrome *c* peroxidase investigated by [^{15}N , ^1H] heteronuclear NMR spectroscopy. *Biochemistry* 40:7069–7076